A High-Precision Land-Sea Segmentation Model Based on the Deep Otsu Method

Tengteng Dong[1*], Mi Wang[1], Tiyou Zhou[1], Qianyu Wu[1]

[1]State Key Laboratory of information Engineering in Surveying, Mapping and Remote Sensing(LIESMARS), Wuhan University, Wuhan 430072, China

Keywords: Land-sea segmentation; Texture enhancement; Deep learning; Maximum inter-class variance method; Pixel clustering

ABSTRACT:
Land-sea segmentation is crucial for tasks such as marine target detection and coastline extraction in remote sensing imagery. However, complex and diverse background environments and land-sea boundaries can easily lead to inaccurate segmentation. To address this issue, a high-precision land-sea segmentation model based on the deep Otsu method is proposed. This method first utilizes our proposed remote sensing image texture enhancement algorithm based on Retinex theory and the Canny operator to enhance the remote sensing image and its edge information, further improving the segmentation accuracy of the land-sea boundary. Then, we combine deep learning concepts, the maximum inter-class variance method, and our proposed density space clustering method based on the difference innovation optimization algorithm to propose a deep maximum inter-class variance method for segmenting the ocean and land in the image. Simultaneously, an adaptive multi-scale fragmentation region removal method is proposed to remove small, fragmented regions extracted during the segmentation process. Experimental results show that the proposed method achieves an overall prediction accuracy of 98.41% and an average intersection-union ratio of 96.07%, demonstrating its ability to effectively perform land-sea segmentation tasks.

1. INTRODUCTION

Land-sea segmentation is an important step in applications such as ship target detection and coastline extraction (Li et al., 2019; Yang et al., 2004; Xing et al., 2015). Accurate land-sea segmentation can remove interference from strong scattering centers in land areas, effectively reduce the false alarm rate of marine target detection, and improve detection efficiency. Currently, there is a lot of work on land-sea segmentation of optical remote sensing images, such as land-sea segmentation methods based on land-sea boundary tracking (Li et al., 2014), land-sea segmentation methods based on coastline databases (Zhang et al., 2020), and methods using pixel feature learning (Wang et al., 2017). In addition, deep neural networks have also been widely used in land-sea segmentation tasks in recent years (Cui et al., 2020). However, optical remote sensing images are easily limited by weather conditions such as clouds and fog, and have insufficient applicability in complex marine monitoring scenarios, which has made land-sea segmentation of synthetic aperture radar (SAR) images a research hotspot (Dai et al., 2020). SAR technology has the ability to work in all weather conditions and its data shows unique advantages in ship detection and coastal zone management, but the speckle noise and strong scattering characteristics of SAR images lead to poor generalization and cumbersome parameter adjustment problems in traditional threshold segmentation, clustering and other methods (Wei et al., 2020). To this end, researchers have adapted deep learning models to SAR image processing. For example, Dai Muchen et al., 2020 proposed an improved bilateral network (D-BiSeNet), which optimized the spatial path convolution structure and edge enhancement loss function to achieve a high-resolution SAR image segmentation accuracy of 0.9889 and a processing speed of 12.7 frames/s (Dai et al., 2020). Wei et al., 2020 embedded the land-sea segmentation module into a cascaded detection framework, which effectively reduced the false alarm rate of ship detection in complex large scenes by strengthening the extraction of spatial location information (Wei et al., 2020).

In terms of model architecture innovation, attention mechanism and multi-scale feature fusion have become breakthrough directions. The dual attention mechanism model proposed in (Ji et al., 2025) significantly improved the segmentation accuracy of coastline boundaries by co-coding convolutional block attention and efficient multi-head attention, combined with an adaptive feature fusion decoding module (Li et al., 2024). The latest research of SPIE is based on Res2Net to build a multi-scale U-Net variant, which integrates channel-space attention and multi-dilation rate convolution, and verified the segmentation robustness of complex coastline areas on the Landsat-8 dataset (Li et al., 2025). In addition, multi-source data fusion technology provides a new approach for land-sea segmentation. Ji et al. effectively eliminated the missegmentation caused by isolated regions by combining grayscale, gradient and texture features through multi-dimensional analysis (Ji et al., 2025).

Despite significant progress in research, current methods still face multiple challenges: the fuzzy boundary of complex coastal zones (such as multiple islands and mudflats) leads to a decrease in segmentation accuracy (Li et al., 2025), lightweight models have bottlenecks in maintaining a balance between accuracy and efficiency (Dai et al., 2020), and the inconsistency of spatiotemporal benchmarks and feature heterogeneity of multi-source data also increases the difficulty of fusion (Ji et al., 2024). At the same time, the dependence of deep learning models on labeled samples and the sensitivity of small target area segmentation have not been fully resolved (Wei et al., 2020). While these methods have advanced the field, they often leave legacy issues, such as the potential loss of fine edge details during the removal of fragmented regions or failure cases in scenarios where land-sea grayscale contrast is extremely low. Therefore, in view of the problem that complex and diverse background environments and land-sea boundaries are prone to inaccurate land-sea boundary segmentation, a high-precision land-sea segmentation model based on the deep Otsu method is proposed.

This contribution has been peer-reviewed. The double-blind peer-review was conducted on the basis of the full paper.
https://doi.org/10.5194/isprs-annals-XI-3-2026-531-2026

This method first uses the remote sensing image texture enhancement algorithm based on Retinex theory and Canny operator proposed by us to enhance the remote sensing image and its edge information, further improving the segmentation accuracy of land-sea boundaries. Next, we combine deep learning concepts, the Otsu's method, and our proposed density space clustering method based on the differential innovation optimization algorithm to propose a deep Otsu's method for segmenting ocean and land in images. Simultaneously, we propose an adaptive multi-scale fragmentation removal method to remove extracted small-area fragmented regions. The main contributions of this method are as follows:

a. We propose a remote sensing image texture enhancement algorithm based on Retinex theory and the Canny operator to enhance remote sensing images and their edge information, thereby further improving the segmentation accuracy of land-sea boundaries.
b. We combine deep learning concepts, the Otsu's method, and our proposed density space clustering method based on the differential innovation optimization algorithm to propose a deep Otsu's method for segmenting ocean and land in images.
c. We propose an adaptive multi-scale fragmentation removal method to remove extracted small-area fragmented regions.

2. METHOD

This paper addresses the problem of inaccurate sea-land boundary segmentation caused by complex and diverse background environments and the inherent challenges of sea-land boundaries. A novel sea-land segmentation algorithm is designed to achieve high-precision and rapid sea-land segmentation, providing effective support for subsequent applications such as ship detection and coastline extraction. The overall algorithm flow is shown in Figure 1, and its details will be explained below.

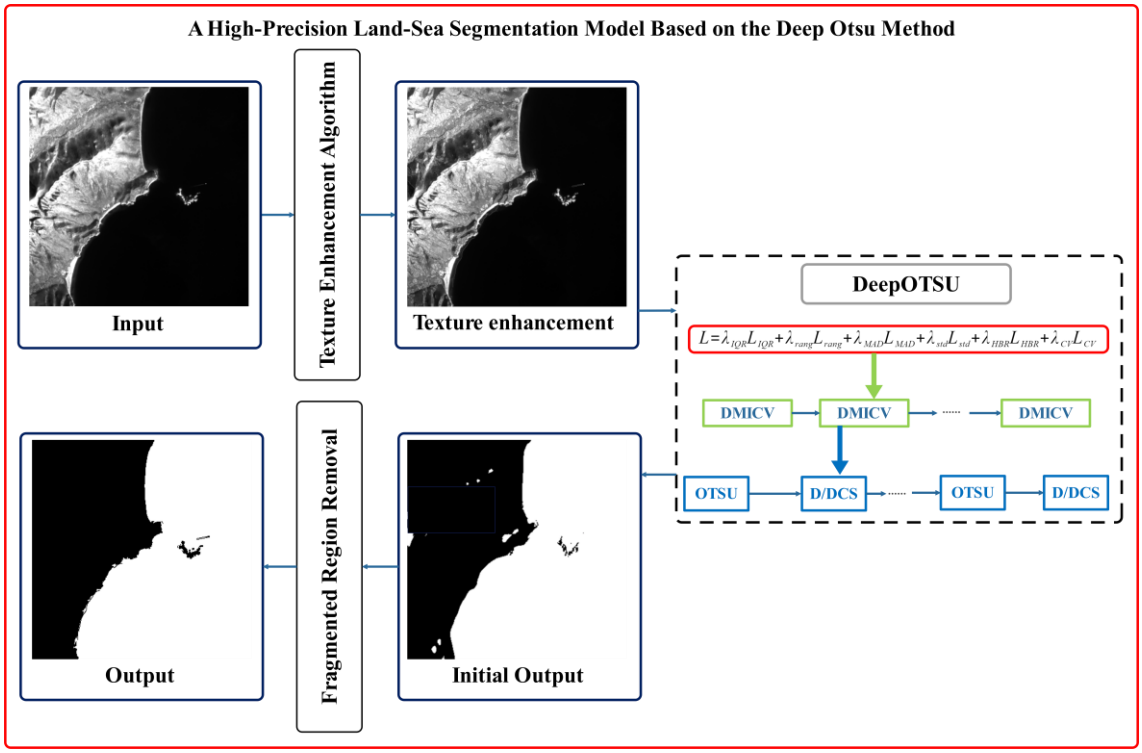

Fig.1 A high-precision land-sea segmentation model based on the deep Otsu method

2.1. Texture Enhancement

In order to further improve the segmentation accuracy of the land-sea boundary, before land-sea segmentation, we use the proposed remote sensing image texture enhancement algorithm based on Retinex theory and Canny operator to enhance the remote sensing image and its edge information.

We first use the algorithm based on Retinex theory to enhance the image and restore the weaker texture information in the image. The purpose of image enhancement based on Retinex theory is to estimate the illumination map L from the original image I, according to $R = \frac{I}{L}$, decompose it to obtain R, and R is the desired enhanced image. The problem of obtaining the illumination map L can be regarded as an optimization problem. Given a grayscale image I and its corresponding normalized image $N = \|I\|$, the illumination map L can be obtained by minimizing the following weighted least squares formula $J(L)$ to obtain the illumination map L:

$$J(L) = \sum_p \left((L_p - N_p)^2 + \lambda \sum_{q \in N(p)} w_{p,q}(I) (L_p - L_q)^2 \right) \quad (1)$$

In this equation, $p = (x, y)$, $0 \le x \le W$, $0 \le y \le H$ is the pixel position, Wis the width of imageI, H is the height. $N(p)$ represents the neighboring positions of p (4*4 window). λ is a control parameter, the larger the value, the smoother the output illumination map L. We generally set it to 15. $w_{p,q}(I)$ is a weight function, which is a Gaussian function, defined as:

$$w_{p,q}(I) = exp\left(\frac{-(I_p - I_q)^2}{\sigma} \right) \quad (2)$$

exp is an exponential function; σ is a control parameter, generally set to 10. The role of the weight function is to give a smaller weight value to pixels with high gradient values (object edges), and a larger weight value to pixels with low gradient values. With this setup, in the illumination map L obtained by minimizing J, the object edges are preserved, while the other textures are smoothed.

After solving (1), the illumination map L can be obtained, and then the enhanced image R can be obtained according to $R = \frac{I}{L}$. In order to adjust the brightness of R, we perform a gamma correction on the illumination map L, so that $R = \frac{I}{L^{\gamma}}$. Here, we generally set γ between 0.5 to 0.7.

After obtaining the enhanced image R, we use the Canny operator to extract and enhance the edge texture information of the enhanced image R to obtain the final edge enhanced image R, as shown in Figure 2.

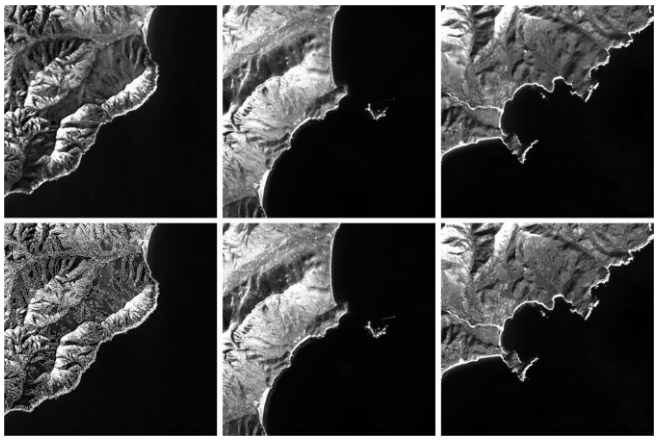

Fig.2 Texture enhancement results.

2.2. Sea-Land Segmentation Method Based on DeepOTSU

DeepOTSU is a pixel classification framework developed by integrating deep learning principles, the Otsu thresholding method, and the newly proposed Differentiated Creative Search-based DBSCAN (DCS-DBSCAN). The architecture primarily comprises the Otsu component and the DCS-DBSCAN module. Its specific structural configuration is illustrated in Figure 3.

2.2.1. OTSU: Maximum Inter-Class Variance Method

The maximum inter-class variance method, commonly referred to as Otsu’s method (Otsu, 1975), operates on the fundamental principle of utilizing an optimal threshold to bifurcate image data into two distinct categories: the background and the target. Within this framework, pixels are partitioned such that one class contains grayscale values strictly below the threshold, while the other encompasses values greater than or equal to the threshold. The optimal threshold is identified when the variance between these two classes is maximized, signifying a clear distinction between the image components.

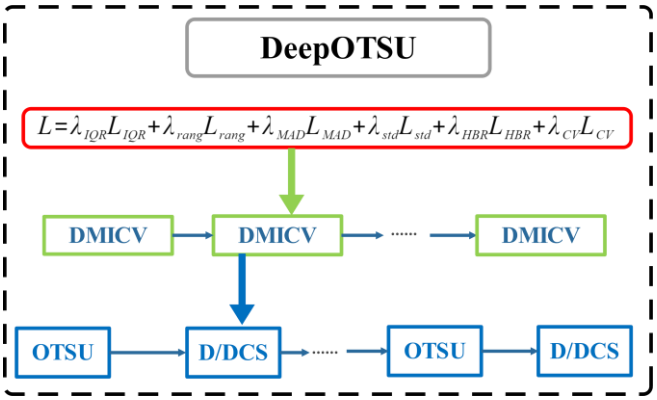

Fig.3 DeepOTSU: A pixel classification module proposed by combining deep learning concepts, OTSU, and our proposed DCS-DBSCAN.

Let the image dimensions be defined as $M \times N$ and the optimal segmentation threshold be denoted as T. The number of pixels categorized as background is N_0, while the target pixels are denoted as N_1. The background proportion is represented by ω_0 with a mean grayscale value of μ_0, and the target proportion is ω_1 with a mean grayscale value of μ_1. The global mean grayscale value of the image is denoted as μ. These relationships are mathematically expressed as follows:

$$\omega_0 = \frac{N_0}{M \times N}, \omega_1 = \frac{N_1}{M \times N}, N_0 + N_1 = M \times N \quad (3)$$

Consequently, it follows that:

$$\omega_0 + \omega_1 = 1, \mu = \frac{\mu_0 * N_0 + \mu_1 * N_1}{M \times N} \quad (4)$$

As established by Otsu (1975), the within-class variance $\sigma_W^2 = \omega_0\sigma_0^2 + \omega_1\sigma_1^2$ and the between-class variance $\sigma_B^2 = \omega_0\omega_1(\mu_0 - \mu_1)$ are defined, where σ_0^2 and σ_1^2 represent the variances of the background and target pixels, respectively. Theoretically, ideal segmentation occurs when the within-class variance is minimized and the between-class variance is maximized, indicating significant differentiation between the background and target segments. Therefore, the optimal threshold T is obtained through a traversal method to maximize the between-class variance.

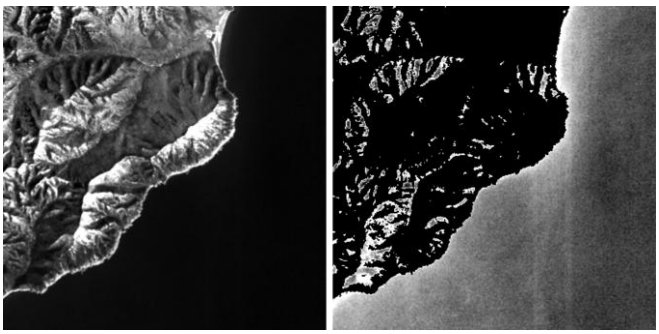

（a） （b）

Fig.4 OTSU classification results: (a) original image, (b) OTSU classification results

This contribution has been peer-reviewed. The double-blind peer-review was conducted on the basis of the full paper.
https://doi.org/10.5194/isprs-annals-XI-3-2026-531-2026 | © Author(s) 2026. CC BY 4.0 License.

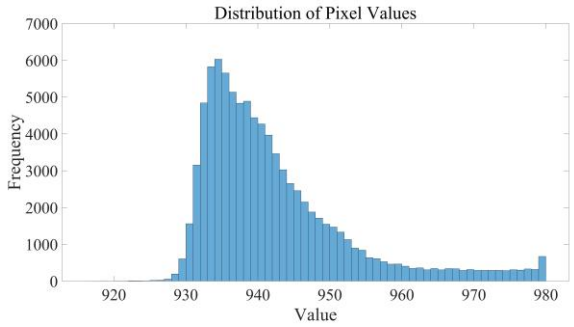

Fig.5 Pixel distribution of classification results

However, the application of standard Otsu thresholding for pixel classification exhibits substantial limitations: it is restricted to binary classification and often suffers from low accuracy, leading to the inclusion of heterogeneous pixels within the identified categories. In this study, Otsu’s method was applied to the remote sensing image in Figure 4a, resulting in the classification shown in Figure 4b. Statistical analysis of Figure 4b, presented in the histogram in Figure 5, reveals that while pixels are primarily concentrated between 930 and 953, the results still contain a significant volume of misclassified outlier pixels.

2.2.2. DCS-DBSCAN: Density Space Clustering Method Based on The Differentiated Creative Search Algorithm

To address the precision limitations of Otsu's method, the DCS-DBSCAN algorithm is employed to eliminate anomalous pixels from the initial classification results. The conventional DBSCAN algorithm (Ester et al., 1996) relies on two critical parameters: the maximum neighborhood radius ϵ and the minimum number of points $MinPts$ to define data density and isolate noise. The selection of these parameters, based on the specific characteristics of the dataset, is decisive for the resulting clustering performance. Consequently, this paper utilizes the Differentiated Creative Search (DCS) algorithm to optimize these parameters, ensuring the most effective data clustering analysis. The proposed DCS-DBSCAN method serves to refine the Otsu classification by removing noise and outliers.

The implementation of DCS-DBSCAN for outlier removal involves the following primary steps:

1) **Construction of the Fitness Function:** The silhouette coefficient is selected as the fitness function to evaluate the clustering quality. This metric assesses the clarity of the cluster outlines by considering two factors: compactness (intra-class closeness) and separation (inter-class distance). The silhouette coefficient ranges from $[-1,1]$, where values approaching 1 indicate superior clustering, while values near -1 signify poor performance. For a single sample i, the silhouette coefficient $s(i)$ is:

$$s(i) = \frac{b(i)-a(i)}{max\{a(i),b(i)\}} \tag{5}$$

where $a(i)$ is the average distance to other samples in the same cluster A, and $b(i)$ is the minimum average distance to samples in other clusters B. The global silhouette coefficient S is the average of all N samples:

$$S = \frac{1}{N}\sum_{i=1}^{N} s(i) \tag{6}$$

where N is the total number of samples.

2) **DCS optimization:** Following the methodology described by Duankhan et al. (2024), the DCS algorithm is applied to maximize the fitness function S. This process yields the optimal values for ϵ and $MinPts$, which are critical for the removal of anomalous pixels.

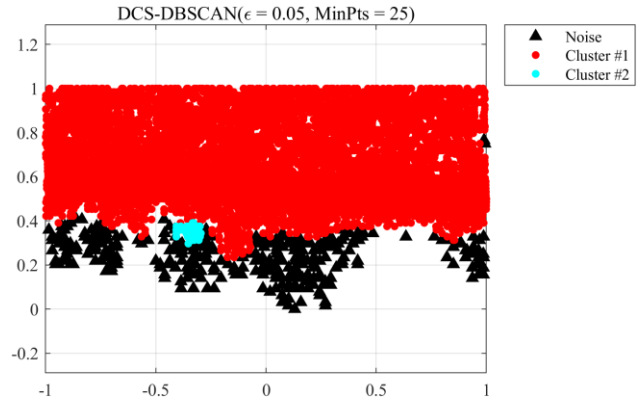

Fig. 6 DCS-DBSCAN clustering result map

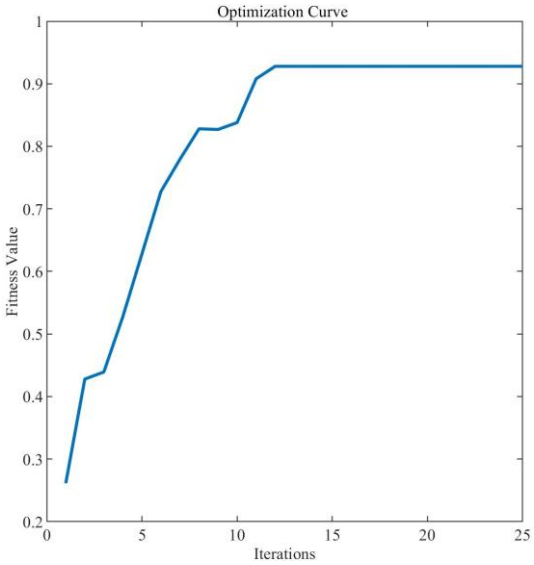

Fig. 7 DCS optimization curve

3) **DCS-DBSCAN clustering:** The optimized parameters are applied to the pixel set to identify the cluster structure and process outliers. After normalizing the classification results from Figure 4 to a range of $[-1,1]$, DCS-DBSCAN was applied. The resulting clustering and the DCS optimization curve are shown in Figure 6 and Figure 7, respectively. The results demonstrate that DCS-DBSCAN offers high accuracy and stability. It effectively captures the internal structure of the pixel set, providing a reliable foundation for subsequent outlier removal.

2.2.3. Sea-Land Segmentation

To achieve high-precision sea-land segmentation, an iterative refinement approach is proposed. In each iteration, DCS-DBSCAN processes the Otsu classification results to remove noise and the smallest pixel clusters. A multi-component loss function is introduced to evaluate whether the optimal segmentation has been reached:

$$L = \lambda_{IQR}L_{IQR} + \lambda_{rang}L_{rang} + \lambda_{MAD}L_{MAD} + \lambda_{std}L_{std} + \lambda_{HBR}L_{HBR} + \lambda_{CV}L_{CV} \tag{7}$$

where L_{IQR}、L_{rang}、L_{MAD}、L_{std}、L_{HBR} and L_{CV} represent the interquartile range, range, mean absolute difference, standard deviation, variation ratio, and coefficient of variation, respectively. These metrics characterize data dispersion. Lower absolute values indicate higher data concentration. The smaller the absolute value of the above indicators, the more concentrated the data. λ_{IQR}、λ_{rang}、λ_{MAD}、λ_{std}、λ_{HBR} and λ_{CV} are the weight coefficients corresponding to the above indicators, and they are of the same size.

$$L_{IQR} = Q_3 - Q_1 \tag{8}$$

$$L_{rang} = Xmin_{max} \tag{9}$$

$$L_{MAD} = \frac{\sum_{i=1}^{n}(X-\overline{X})}{n} \tag{10}$$

$$L_{std} = \sqrt{\frac{\sum_{i=1}^{n}(X-\overline{X})^2}{n}} \tag{11}$$

$$L_{HBR} = \frac{n-f_m}{n} \tag{12}$$

$$L_{CV} = \frac{\sqrt{\frac{\sum_{i=1}^{n}(x-\overline{X})^2}{n}}}{\overline{X}} \tag{13}$$

Where Q_1, Q_2, and Q_3 are the three points that divide all the data into four equal parts after sorting a group of data of length n. The values corresponding to the positions of these three points are called quartiles, which are recorded as Q_1 (first quartile), Q_2 (second quartile), and Q_3 (third quartile). X_i is the element in the array, $\overline{X}$ is the mean of the array, and f_m is the number of the mode in the array.

Algorithm 1 Sea-Land Segmentation Method Based on DeepOTSU

Input：Input image Y
Initialize：$i = 0$
1：While Y is not empty
2：$T^0 = OTSU(Y)$
1：Obtain the initial classification result O^0 based on the segmentation threshold T^0
2：Calculate the initial loss function L^0 based on the initial classification result O^0
3：Do DeepOTSU：
4：While True
5：$DCS - DBSCAN(O^i)$
6：$T^{i+1} = OTSU(O^i)$
7：$O^{i+1} = O^i(O^i < T^{i+1})$
8：$L^{i+1} = L(O^{i+1})$
9：$i++$
10：If L^{i+1} stabilizes the loop ends
11：Get the optimal segmentation threshold T and a certain pixel classification result O_j
Output：Sea-Land Segmentation Result O_j

When the loss function L stabilizes, the anomalous pixels are considered eliminated, and the resulting Otsu threshold is deemed optimal. This optimal threshold is then applied for final sea-land segmentation in remote sensing imagery. The full procedure is summarized in Algorithm 1.

2.3. Fragmented Region Removal

Due to the influence of factors such as sun elevation angle and imaging angle during the imaging process of remote sensing images, there may be shadow areas in the obtained images. The existence of these shadow areas will adversely affect the accuracy of land-sea segmentation, often resulting in some fragmented regions similar to the sea in the segmentation results. In addition, some small-area waters may also be misidentified as the sea and extracted, adversely affecting the segmentation accuracy. To this end, we propose an adaptive multi-scale fragmented region removal method to remove the extracted small-scale fragmented regions.

The core of the fragmented region removal method proposed in this paper lies in removing the fragmented regions by statisticsing whether the proportion of the extracted sea pixels in windows of different scales reaches the set threshold. The threshold size is inversely proportional to the window size, and will increase gradually as the window size decreases, as shown in the following formula:

$$P_{i,j} = \frac{\phi}{D} \tag{14}$$

Through extensive experiments, this method can effectively remove the fragmented regions extracted under the influence of sun elevation angle, imaging angle and small-area waters, further improving the accuracy of land-sea segmentation.

Tab.1 Comparison of segmentation performance of different methods on HY-1E data.

Methodologies	MIoU/%	OA/%	Mmed/unit pixel
CCNet	72.067	74.158	89.792
PSPNet	86.293	88.724	65.307
U-Net	85.080	86.537	57.903
Ours	96.067	98.413	10.476

3. EXPERIMENTAL RESULTS AND ANALYSIS

To verify the effectiveness of the proposed method, we utilized multispectral imagery data captured by the Coastal Zone Imager (CZI) carried by the new-generation ocean color observation research satellite HY-1E. The core technical specifications of the acquired imagery are listed as follows: the nadir ground pixel resolution is ≤ 20 m, the swath width is ≥ 60 km, and the observable range extends to ≥ 1,000 km under side-swing conditions. This sensor is primarily tailored for coastal zone environmental monitoring and automatic ship recognition tasks. Notably, the land-sea segmentation method developed in this study offers robust technical support for the practical application of HY-1E satellite coastal zone imagery. To further validate its performance superiority, comparative experiments were conducted between the proposed method and three state-of-the-art land-sea segmentation approaches reported in recent years. Corresponding experimental results are presented in Figure 8.

It can be seen from Figure 8 that the CCNet (Huang et al., 2019), PSPNet (Zhao et al., 2017), and U-Net (Zhou et al., 2021) methods all show hollow effects in inland areas, while in ocean areas, the CCNet and PSPNet methods wrongly segment low-brightness areas on land as ocean areas. In contrast, the method in this paper has relatively superior segmentation effects in both land and ocean areas, with fewer missegmentation areas. In addition, due to the lack of edge area information, the segmentation accuracy of the CCNet and PSPNet methods in the land-sea boundary area is also lower. Although the accuracy of the method in this paper is higher, there are still some problems such as insufficient fineness of details in a small number of regional edges, which is specifically manifested as small protrusions or depressions on the edges that may be smoothed out. The reason may be that some edge information was destroyed when removing fragmented regions. However, just from the visual

effect, the method in this paper has achieved the optimal land-sea segmentation results.

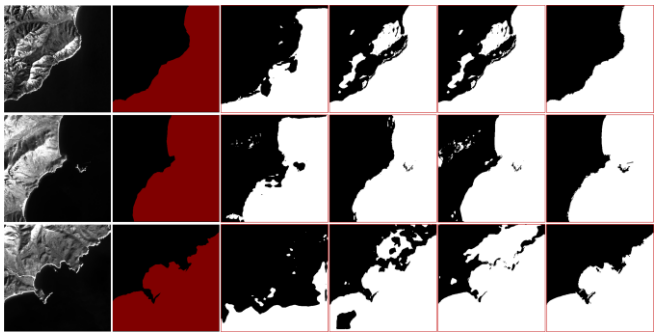

Fig.8 Segmentation results of different methods: From left to right, input images, labels, CCNet, PSPNet, U-Net, Ours.

In order to better analyze the accuracy and superiority of the algorithm in this paper, we used 100 HY-1E images to calculate the mean Intersection over Union (mIoU), overall accuracy (OA) and mean Minimum Boundary Distance (mMED) of each method, and further compared the land-sea segmentation results of the above methods. The comparison results are shown in Table 1. It can be seen from Table 1 that the mIoU, OA and mMED of the method in this paper are superior to traditional methods, especially in the mMED metric a significant advantage is achieved.

Tab.2 The average time (T, s) required to perform land-sea segmentation on the image shown in Figure 8.

Methodologies	CCNet	PSPNet	U-Net	Ours
T	0.45	0.67	0.84	13.27

To provide a more comprehensive evaluation of the proposed framework, we analyzed the computational efficiency of each algorithm, defined as the average processing time required to process the three images illustrated in Figure 8. The results are summarized in Table 2. Although the proposed method does not achieve the highest execution efficiency, this is primarily attributed to the time consumed by the DCS algorithm in determining the optimal ϵ and $MinPts$ values during the search for the ideal segmentation threshold. However, the sea-land segmentation performance of the proposed method significantly outperforms the benchmark methods. It achieves complete separation of marine and terrestrial regions without compromising the integrity of the sea-land boundaries. This superiority is clearly demonstrated by the segmentation results and various quantitative evaluation metrics, as shown in Figure 8 and Table 1, respectively.

4. CONCLUSION

This paper proposes a high-precision land-sea segmentation model based on the deep Otsu method to achieve land-sea segmentation of remote sensing images in complex scenarios. The model first enhances the remote sensing image and its edge information using a proposed remote sensing image texture enhancement algorithm. Then, it uses the proposed deep Otsu method to segment the ocean and land in the image. Simultaneously, an adaptive multi-scale fragmentation region removal method is proposed to remove small, fragmented regions extracted from the image. Experiments using HY1E satellite imagery demonstrate that the proposed method outperforms current mainstream semantic segmentation networks in both region and edge segmentation accuracy, and can effectively complete the land-sea segmentation task.

REFERENCES

Cui, B., Jing, W., Huang, L., Li, Z., & Lu, Y. (2020). SANet: A sea–land segmentation network via adaptive multiscale feature learning. IEEE Journal of Selected Topics in Applied Earth Observations and Remote Sensing, 14, 116-126.

Duankhan, P., Sunat, K., Chiewchanwattana, S., & Nasa-Ngium, P. (2024). The Differentiated Creative Search (DCS): Leveraging differentiated knowledge-acquisition and creative realism to address complex optimization problems. Expert systems with applications, 252, 123734.

Dai, M., Leng, X., Xiong, B., & Ji, K. (2020). Sea-land segmentation method for SAR images based on improved BiSeNet. Journal of Radar, 9(5), 886-897.

Ester, M., Kriegel, H. P., Sander, J., & Xu, X. (1996). Density-based spatial clustering of applications with noise. In Int. Conf. knowledge discovery and data mining, 240, 6.

Huang, Z., Wang, X., Huang, L., Huang, C., Wei, Y., & Liu, W. (2019). Ccnet: Criss-cross attention for semantic segmentation. In Proceedings of the IEEE/CVF international conference on computer vision, 603-612.

Ji, Y., Shi, W., Lei, J., & Ding, J. (2025). DBRSNet: a dual-branch remote sensing image segmentation model based on feature interaction and multi-scale feature fusion. Scientific Reports, 15(1), 27786.

Ji, Y., Wu, W., Nie, S., Wang, J., & Liu, S. (2024). Sea–land segmentation of remote-sensing images with prompt mask-attention. Remote Sensing, 16(18), 3432.

Li, C., Pan, Q., Zhang, Z., Liu, Z., Bai, X., & Pan, K. (2024, July). Land-Sea Clutter Classification for Over-the-Horizon Radar via Dual Attention Aided Residual Neural Networks. In 2024 27th International Conference on Information Fusion (FUSION) (pp. 1-7). IEEE.

Li, W., & Gao, J. (2025, June). A multiscale land-sea segmentation method based on U-Net. In International Conference on Remote Sensing, Surveying, and Mapping (RSSM 2025) (Vol. 13642, pp. 713-718). SPIE.

Otsu, N. (1975). A threshold selection method from gray-level histograms. Automatica, 11, 285-296.

Wang, D., Cui, X., Xie, F., Jiang, Z., & Shi, Z. (2017). Multi-feature sea–land segmentation based on pixel-wise learning for optical remote-sensing imagery. International journal of remote sensing, 38(15), 4327-4347.

Wei, S., Su, H., Ming, J., Wang, C., Yan, M., Kumar, D., ... & Zhang, X. (2020). Precise and robust ship detection for high-resolution SAR imagery based on HR-SDNet. Remote Sensing, 12(1), 167.

Wang, J., Lu, C., & Jiang, W. (2018). Simultaneous ship detection and orientation estimation in SAR images based on attention module and angle regression. Sensors, 18(9), 2851.

Xing, X., Ji, K., Kang, L., & Zhan, M. (2015). A review of research on ship target surveillance technology using HRWS SAR images. Journal of Radar, 4(1), 107-121.

Xu, S., Bai, X., Ren, Q., & Li, D. (2023). Sea–Land Segmentation Algorithm Based on Multiframe Radar Echoes. IEEE Transactions on Geoscience and Remote Sensing, 61, 1-10.

Yang, W., Sun, H., Xu, X., & Xu, Ge. (2004). Ship and track detection in spaceborne SAR images. Journal of Wuhan University: Information Science Edition, 29(8), 682-685.

Zhang, J., Jing, H., & Fan, S. (2020). Land-sea segmentation of remote sensing images based on coastline database. Electronic Measurement Technology, 43(23), 115-120.

Zhao, H., Shi, J., Qi, X., Wang, X., & Jia, J. (2017). Pyramid scene parsing network. In Proceedings of the IEEE conference on computer vision and pattern recognition (pp. 2881-2890).

Zhou, Y., Zheng, G., Yang, J., Li, X., Liu, B., Shao, J., ... & Zhang, B. (2021, November). Sea-land segmentation of synthetic aperture radar imagery using deep neural network models. In 2021 Photonics & Electromagnetics Research Symposium (PIERS) (pp. 2006-2010). IEEE.